Improved electrochemical performance in Sc-doped nanocrystalline $LiMn_2O_4$

Victor Gin He Leong, Seung Sae Hong, Ricardo H. R. Castro*

Department of Materials Science and Engineering, University of California–Davis, One Shields Avenue, Davis, CA 95616, United States

*Corresponding Author: rhrcastro@ucdavis.edu

Abstract

Jahn-Teller effects have been widely known to cause capacity fading in $LiMn_2O_4$ (LMO) cathode materials due to Mn dissolution from the cathode/electrolyte interfaces. This effect is more pronounced in nanoscale materials due to their high surface reactivity. Although surface coatings can help mitigate the phenomenon, there is still limited understanding of the correlation between the spontaneous segregation of dopants to interfaces and the cathode electrochemical performance. This work demonstrates that an interfacial dopant, Sc^{3+}, selected on a thermodynamic principle, segregates to surfaces and grain boundaries and acts as a system stabilizer. The electrochemical performance in Li/LMO half-cells showed nanostructured Sc^{3+}-doped LMO delivers capacity retention of 97.3% after 50 cycles at 0.2C compared to an equivalent undoped LMO with only 88.3%. Sc-doping reduces the charge transfer resistance while maintaining its high characteristic diffusion coefficient (D_{Li+}) of 9.089×10^{-11} cm^2/s. The work highlights that understanding the thermodynamic stabilization of cathode materials can provide a pathway to advance cathode technologies even beyond Lithium.

Keywords: Interface, thermodynamics, $LiMn_2O_4$, nanoparticles

1. Introduction

$LiMn_2O_4$ (LMO) is a competitive cathode material for Li-ion batteries due to its low cost, natural abundance of Mn, and low toxicity compared to the dominant chemistry, $LiCoO_2$.[1] Nanostructured LMO offers further advantages with shorter diffusion paths, which allow for higher charge and discharge rates.[2–4] However, LMO shows instabilities related to Jahn-Teller distortions severed by the dissolution of Mn ions in hydrofluoric acid and the electrolyte.[5] These and other parasitic reactions cause structural volume changes during cycling, inducing intergranular cracking at the cathode or cathode-electrolyte interface. These problems are augmented in the nanoscale systems due to their intrinsic high interfacial areas and respective reactivity, accelerating cell capacity fade. [4]

The instability of nanomaterials is associated with the increased excess energies from the high fraction of atoms in the interfacial regions [6–8]. The local energies can be reduced by designing the composition to allow spontaneous ion segregation [8]. Based on the Gibbs adsorption isotherm formalism, surface excess (or segregation) of ions will decrease the interfacial energies proportionally to the excess amount and the segregation energy [9,10]. Recently, Sc^{3+} introduced in LMO successfully reduced the system's surface energy from 0.85 J/m^2 to 0.48 J/m^2 (for reference, surface energy for $LiCoO_2$ is 1.12 J/m^2 [11]). The values represent a significant reduction in coarsening driving force and were expected, yet not tested, to improve cathode stability during cycling by reducing reactivity. The present work explores the potential improvements in electrochemical performance in Sc^{3+}-doped LMO and demonstrates that segregation is a promising mechanism for improving nanostability in battery systems.

2. Experimental Section

LMO nanoparticles were synthesized using a custom-built flame spray pyrolysis system (FSP). Details of the synthesis are in the Supplemental Information. The crystallographic phases and sizes were determined using X-ray diffraction (XRD, Bruker AXS Inc., Madison, WI, USA) with a scan range of 15˚ to 90˚ and Cu K-alpha radiation and 40kV, 40mA. The surface areas were analyzed using Brunauer-Emmet-Teller (BET) method in a Gemini VII Surface Area Analyzer (Micromeritics Instrument Corp., Norcross, GA, USA). The spatial distribution of Sc^{3+}-doped LMO was studied using scanning transmission electron microscopy (STEM) at 200kV coupled with energy electron loss spectroscopy (EELS) using JEOL 2100F (S)TEM and a Gatan Tridiem Spectrometer. Grain sizes measured in STEM were consistent with crystallite sizes from XRD pattern refinements.

A Li-ion electrochemical coin-cell (CR2032) was used to evaluate the electrochemical cyclic charge/discharge performance of the cathodes. Details of cell fabrication are in Supplemental Information. Cells were cycled at 0.1C from 3.0V to 4.2V to ensure uniform growth of the SEI layer. The cycles were performed using BT2000 Arbin Potentiostat with the same voltage range and C-rates of 0.2C for both compositions. Gamry 1010E was used to measure the cell's impedance at the 50^{th} cycle with amplitude voltage 5mV, and frequency range 500 kHz to 0.01 Hz.

3. Results and Discussion

XRD patterns on the as-sprayed powders showed a combination of phases, including Mn_3O_4 and Mn_2O_3 (see Fig. S1). That was attributed to low flame temperatures utilized during the combustion process to reduce coarsening and produce nanoscale particles.[5] Annealing under O_2 successfully converted the material to single-phase LMO with the characteristic spinel structure without significant coarsening.

Table 1. Surface area, crystallite/grain size, and lattice parameter measurements of Sc^{3+}-doped and undoped nanoparticles.

Sample	Avg. Surface Area (m^2/g)	Avg. Grain Boundary Area (m^2/g)	Avg. Grain Size (nm)	Lattice Parameter '*a*' (Å)	Unit Cell Volume ($Å^3$)
LMO	17.1	10.5	43.3	8.229	557.2
Sc -LMO	36.9	27.4	18.0	8.204	552.2

Table 1 shows the crystallite size and lattice parameters calculated from whole profile fitting (shown in Fig. S2) and the BET surface areas (adsorption curves shown in Fig S3). The data indicates Sc^{3+} decreases the crystallite size and consequently increases the surface area of the powders, suggesting stabilization of surfaces by Sc^{3+} [8]. The shrinkage of the unit cell is consistent with a suppression of the Jahn-Teller distortion. [12,13]

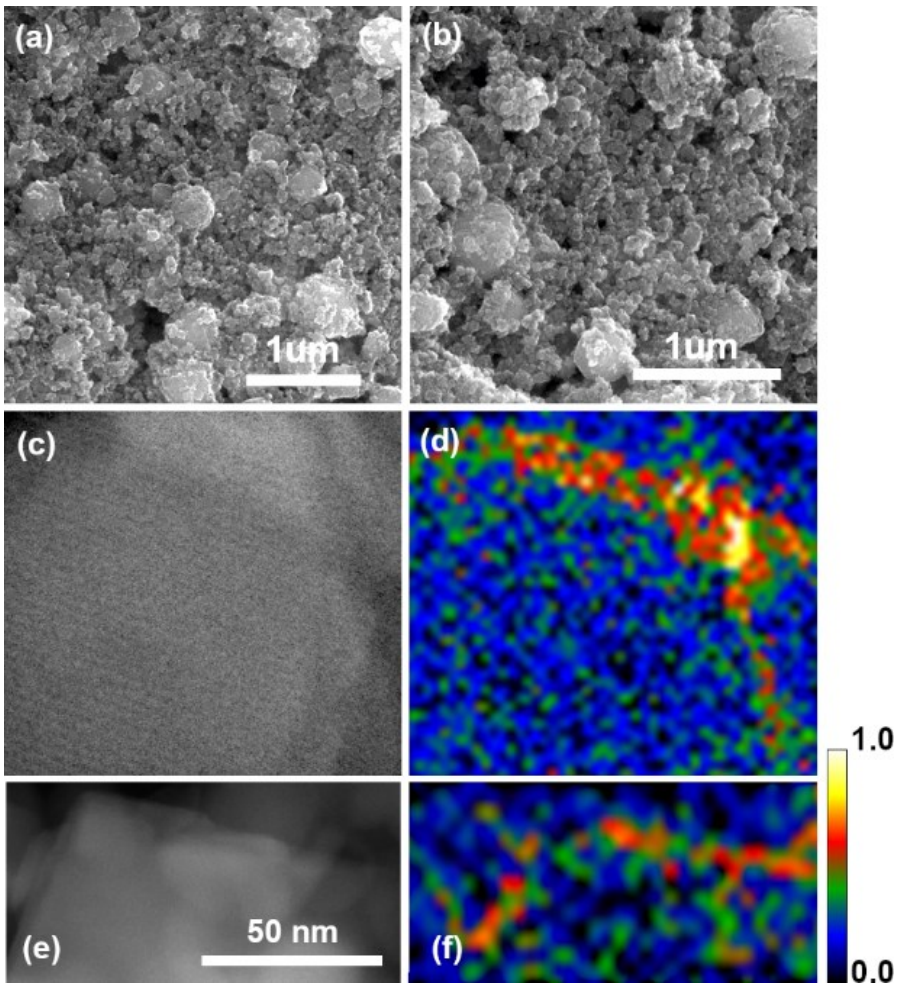

Fig. 1. (a) SEM images for LMO and (b) Sc-doped LMO nanoparticles. (c,e) STEM images of Sc^{3+}-doped LMO nanoparticle, and (d,f) the respective spatial distribution for Sc^{3+} using EELS. Color maps represent the relative concentration of Sc^{3+}. Maps for Mn and O are available in Fig. S5.

Figures 1a and 1b show SEM images revealing LMO nanoparticles are relatively isotropic but agglomerated. Solid-solid interfaces (grain boundaries) inferred by comparing the surface area and the crystallite sizes and assuming tetrakaidekahedra shapes are listed in **Table 1.** Grain boundary area increases with doping, implying stabilization by Sc^{3+}.

Figure 1c-f shows STEM-EELS data evidencing segregation of Sc^{3+} to both interfaces. Fig. 1c shows a survey particle with apparent grain boundaries and the respective EELS mapping indicating localized enrichment (EELS mappings for O and Mn demonstrate evenly distributed elements across the nanoparticles, **Fig. S5**). Fig. 1e shows part of a different particle with clusters on top. The EELS map shows Sc^{3+} enrichment at the surface regions. EELS and STEM images don't perfectly overlap due to shifting during EELS analysis. Nakajima et al. recently reported similar Sc^{3+} segregation in LMO, which resulted in the reduction of both surface and grain boundary energies from γ_s = 0.85 J/m^2 and γ_{GB} = 0.27 J/m^2 for LMO to γ_s = 0.48 J/m^2 and γ_{GB} = 0.24 J/m^2 for Sc^{3+}-LMO [14]. Because here we used 3% Sc^{3+} in contrast to 2% Sc^{3+} reported by Nakajima et al., we used the solute enrichment equation to calculate the energies in our system [6]:

$$\gamma = \gamma_o - \Gamma_B(RT \ln X_B^{bulk} - \Delta H_{seg}) \quad (1)$$

Here, the interfacial energy of the neat system is represented by γ_o, Γ_B is the solute excess, X_B^{bulk} is the solute content in bulk, and ΔH_{seg} is the segregation enthalpy. Calculated energies were γ_s = 0.29 J/m^2 and γ_{GB} = 0.22 J/m^2. The remarkable surface energy reduction is consistent with the increase in interfacial areas in Sc^{3+} doped samples, confirming thermochemistry stabilization.

CR2032 Li-half coins cells were built to investigate the cyclic performance of the nano-cathodes at 0.2C. The LMO cell showed an initial discharge capacity of 89 mAh/g, while the Sc^{3+}-LMO had 78 mAh/g. These are relatively low values attributed to lithium loss during the formation cycle, where lattice reconstruction is expected. However, **Fig. 2b** shows the capacity retention normalized for the initial discharge capacities evidencing Sc^{3+}-LMO cathode with superior capacity retention after 50 cycles.

Electrochemical Impedance Spectroscopy (EIS) using an equivalent circuit shown in **Fig. 2c** revealed that after 50 cycles, R_{SEI} for LMO is slightly higher, suggesting Sc^{3+} hinders the reduction of Mn ions on the SEI interface. Fitting parameters are found in **Table 2**, while the Bode plot and details are in Supplemental Information. R_{ct} of the Sc^{3+}-LMO is maintained significantly lower than LMO even considering the differences in surface areas (**Table 1**), indicating faster kinetics of Li-ions from the cathode and into the electrolyte. The estimated Li^{+} diffusion coefficient of Sc^{3+}-LMO was five times higher than the undoped samples at 3.0V open-circuit voltage. The values are slightly lower than those processed by sol-gel and solid-state synthesized LMO [3], which is related to the lower carbon content.

Table 2. Fitted parameters for EIS study on a half-cell using LMO composite electrode (80:15:5 mass ratio of LMO, carbon black, and poly(tetrafluoroethylene) at 25°C and 3.0V (vs. Li/Li^{+}) obtained via equivalent circuit seen in Fig. 2b. σ is the Warburg coefficient.

Sample	**R_{series} (Ω)**	**R_{SEI} (Ω)**	**R_{ct} (Ω)**	**σ (Ω $s^{-1/2}$)**	**D_{Li+} (cm^2/s)**
LMO	4.877 ± 0.331	8.517 ± 1.116	129.7 ± 2.547	40.177	1.715×10^{-11}
$Sc - LMO$	5.475 ± 0.373	2.411 ± 1.099	26.47 ± 1.200	17.451	9.089×10^{-11}

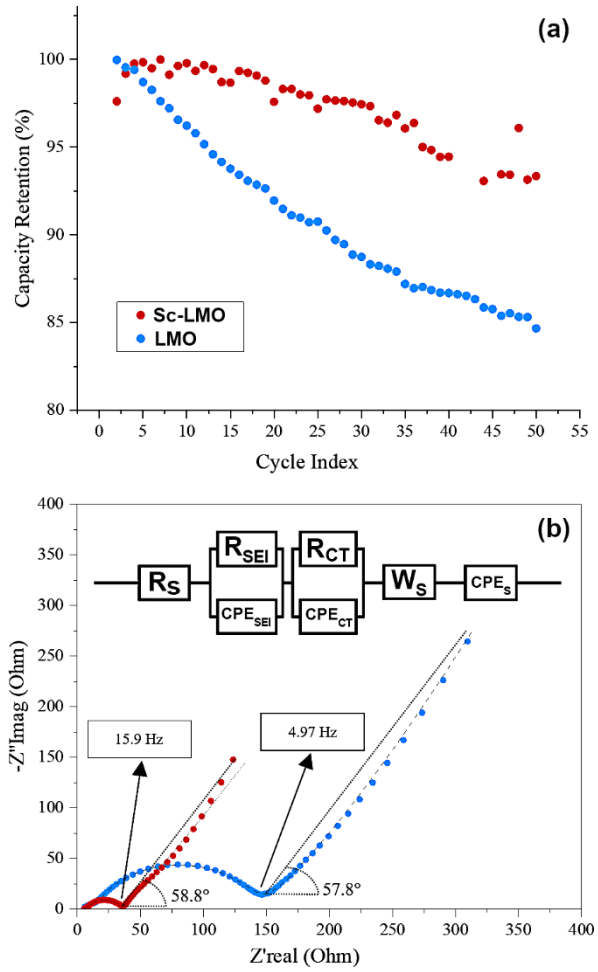

Fig. 2. (a) Normalized capacity retention and (b) EIS spectra for LMO and Sc^{3+}-LMO cells at 50^{th} cycle. The inset represents the resistive model. R_S is the series resistance; R_{SEI} the Solid Electrolyte Interphase Resistance; R_{CT} refers to Charge Transfer Resistance; CPE_{SEI} stands for Solid Electrolyte Interphase Constant Phase Element; CPE_{CT} the Charge Transfer Constant Phase Element; W_s is the Series Warburg; CPE_S the Series Constant Phase Element.

4. Conclusion

Sc^{3+} segregates to the interfaces of LMO nanoparticles, leading to a reduction in excess energies. Half-cell tests showed segregation improves the cycling performance of the nano-cathode and increases charge transfer. Although limited capacity was observed, the data

demonstrate the potential of thermodynamically designing interfaces to expand nano-battery lifetime. We speculate the surface energy reduction suppresses Jahn-Teller distortions by decreasing cathode solubility to improve performance, but more studies are in progress.

5. Acknowledgments

NSF DMR Ceramics 2015650.

References

[1] Y. Lyu, X. Wu, K. Wang, Z. Feng, T. Cheng, Y. Liu, M. Wang, R. Chen, L. Xu, J. Zhou, Y. Lu, B. Guo, An Overview on the Advances of $LiCoO_2$ Cathodes for Lithium-Ion Batteries, Adv. Energy Mater. 11 (2021) 1–29. https://doi.org/10.1002/aenm.202000982.

[2] P.G. Bruce, B. Scrosati, J.M. Tarascon, Nanomaterials for rechargeable lithium batteries, Angew. Chemie - Int. Ed. 47 (2008) 2930–2946. https://doi.org/10.1002/anie.200702505.

[3] X. Cui, S. Du, K. Zhu, S. Geng, D. Zhao, X. Li, F. Tang, S. Li, Elevated electrochemical property of $LiMn_2O_4$ originated from nano-sized Mn_3O_4, Ionics (Kiel). 24 (2018) 697–706. https://doi.org/10.1007/s11581-017-2241-4.

[4] D.K. Kim, P. Muralidharan, H.-W. Lee, R. Ruffo, Y. Yang, C.K. Chan, H. Peng, R.A. Huggins, Y. Cui, Spinel $LiMn_2O_4$ Nanorods as Lithium Ion Battery Cathodes, Nano Lett. 8 (2008) 3948–3952. https://doi.org/10.1021/nl8024328.

[5] G. Zhou, X. Sun, Q.H. Li, X. Wang, J.N. Zhang, W. Yang, X. Yu, R. Xiao, H. Li, Mn Ion Dissolution Mechanism for Lithium-Ion Battery with $LiMn_2O_4$ Cathode: In Situ Ultraviolet-Visible Spectroscopy and Ab Initio Molecular Dynamics Simulations, J. Phys. Chem. Lett. 11 (2020) 3051–3057. https://doi.org/10.1021/acs.jpclett.0c00936.

[6] H. Peng, Z. Jian, F. Liu, Review of thermo-kinetic correlation during grain growth in nanocrystalline materials. Int. J. Ceramic Eng. Sci. 2 (2020) 49– 65. https://doi.org/10.1002/ces2.10040

[7] M.M. Hasan, P.P. Dholabhai, R.H.R. Castro, B.P. Uberuaga, Stabilization of $MgAl_2O_4$ spinel surfaces via doping, Surf. Sci. 649 (2016) 138–145. https://doi.org/10.1016/j.susc.2016.01.028.

[8] R.H.R. Castro, On the thermodynamic stability of nanocrystalline ceramics, Mater. Lett. 96 (2013) 45–56. https://doi.org/10.1016/j.matlet.2013.01.007.

[9] R. Kirchheim, Reducing grain boundary, dislocation line and vacancy formation energies by solute segregation. II. Experimental evidence and consequences, Acta Mater. 55 (2007) 5139–5148. https://doi.org/10.1016/j.actamat.2007.05.033.

[10] D.N.F. Muche, A.L. da Silva, K. Nakajima, D. Gouvêa, R.H.R. Castro, Simultaneous segregation of lanthanum to surfaces and grain boundaries in $MgAl_2O_4$ nanocrystals, Appl. Surf. Sci. 529 (2020) 147145.

[11] P.S. Maram, G.C.C. Costa, A. Navrotsky, Experimental confirmation of low surface energy in $LiCoO_2$ and implications for lithium battery electrodes, Angew. Chemie - Int. Ed. 52 (2013) 12139–12142. https://doi.org/10.1002/anie.201305375.

[12] S. Guo, S. Zhang, X. He, W. Pu, C. Jiang, C. Wan, Synthesis and Characterization of Sn-Doped $LiMn_2O_4$ Cathode Materials for Rechargeable Li-Ion Batteries, J. Electrochem. Soc. 155 (2008) A760.

[13] X. Li, Y. Xu, C. Wang, Suppression of Jahn–Teller distortion of spinel $LiMn_2O_4$ cathode, J. Alloys Compd. 479 (2009) 310–313. https://doi.org/https://doi.org/10.1016/j.jallcom.2008.12.081.

[14] K. Nakajima, F.L. Souza, A.L.M. Freitas, A. Thron, R.H.R. Castro, Improving Thermodynamic Stability of nano-$LiMn_2O_4$ for Li-Ion Battery Cathode, Chem. Mater. 33 (2021) 3915–3925. https://doi.org/10.1021/acs.chemmater.0c04305.